Role of oxygen-containing species at Pt(111) on the Oxygen Reduction Reaction in Acid Media

Ana M. Gómez–Marín*[,a,b] and Juan M. Feliu*[,a]

[a] *Instituto de Electroquímica, Universidad de Alicante, Apt 99, E-03080 Alicante, Spain, Tel.: +34 965 909 301; fax: +34 965 903 537. Email: juan.feliu@ua.es (J.M. Feliu), am.gomez@ua.edu.co (AM Gomez).*

[b] *Eco-Lavka, Cra. 79, #49[a]-30, Medellín, Colombia.*

Abstract:

The oxygen reduction reaction (ORR) is one of the fundamental reactions in electrochemistry and has been widely studied, but the mechanistic details of ORR still remain elusive. In this work, the role of electrochemical oxygenated species, such as adsorbed hydroxide, OH_{ads}, adsorbed oxygen, O_{ads}, and Pt(111) oxide, PtO, in the ORR dynamics is studied by employing electrochemical techniques, *i.e.* combining rotating disk mass-transport control with potential sweep rate perturbation. In this framework, a reduction peak at 0.85 V, E_{ORR}, is detected. This peak shows a different electrochemical dynamics than that of Pt(111) oxides. The data analysis suggests that neither OH_{ads} nor O_{ads} are the main bottleneck in the mechanism. Instead, results support the reduction of a soluble intermediate species as the rate determining step in the mechanism. On the other hand, PtO species, which are generated at relatively high potentials, and are responsible of surface disordering, strongly inhibit the ORR as long as they are adsorbed in the electrode surface.

Keywords: Electrochemical oxygenated species, Pt(111), oxygen reduction reaction, scan rate dynamics, rotating disk electrode.

1. Introduction

The oxygen reduction reaction (ORR) is one of the fundamental reactions in electrocatalysis. It is a multi-electron system that includes several elementary steps and intermediate species [1]. However, despite many years of research, the detailed knowledge of the ORR mechanism remains still unclear. On platinum, the most active pure metal for this reaction, oxygen reduces to water through a four-electron process with a large overpotential, $\eta \sim 0.3$ V [2–6]. This fact has been commonly attributed to a poisoning role of surface platinum oxides [7, 8], however, the exact nature of the inhibitory species has not been determined yet.

Earlier studies reported that the apparent "threshold" potential for ORR is determined by the potential and the rate at which the surface platinum oxide is removed from the electrode surface [7]. In both Pt(poly) [9] and Pt(111) electrodes [10], the Tafel slope changes when the potential is increased from a value where the coverage with oxygen species is virtually zero to a potential region where the surface is oxidized, between 0.8 and 1.0 V. Thus, in general, it is widely accepted that adsorbed hydroxyl, OH_{ads}, or adsorbed oxygen, O_{ads},

are the poisoning species for the reaction. A simple model postulates that OH_{ads} has both site blocking and negative energetic electronic effects and so, the elimination of OH_{ads} would be the rate determining step (RDS) in the ORR mechanism [11–14]. Therefore, ORR kinetics would be determined by the amount of free Pt sites available for O_2 adsorption and the adsorption energy of ORR intermediates [11–22].

In contrast, several works have also reported an enhanced ORR activity due to an increase in the oxygen coverage [23], and smaller improvements than those expected, or even inhibition [24], in the ORR kinetics at lower OH_{ads} coverages [25, 26]. Additionally, hydrogen peroxide reduction, a reaction in which OH_{ads} is also considered to be an intermediate species [27, 28], mostly occurs under mass-controlled conditions, between 0.9 and 0.3 V [28–30]. Hence, if the first step on the ORR mechanism is the formation of O_{ads}, or adsorbed hydroperoxyl radical, OOH_{ads}, as suggested [31, 32], OH_{ads} should not inhibit the process and the identity of the species responsible of the poisoning effect would remain undefined.

Incidentally, once OH_{ads} adsorption on Pt(111) has occurred at the butterfly region in oxygen-free solutions, 0.5-0.9 V, an "extra", reversible adsorption of OH_{ads} at higher potentials is still possible [33], suggesting that OH_{ads} site blocking effect may be unsubstantial. In consequence, if OH_{ads} is not the inhibiting species, estimation of lower OH_{ads} coverages at increased ORR rates [11, 15, 18] would be a circumstantial event, hiding other main possible modifications in the mechanism. This opens the question about the identity of the RDS in the ORR. Moreover, besides OH_{ads}, adsorbed water, H_2O_{ads}, adsorbed oxygen, O_{ads}, and platinum oxides, PtO, also coexist on the surface, in addition to the possible existence of other poisoning adsorbates [26, 34–36], and the effect of these species on the ORR is still not known.

Recently, we have suggested the reduction of a soluble intermediate species as the RDS in the whole reaction mechanism. This intermediate species would be characterized by a new reduction peak around 0.85 V at 0.05 V s^{-1}, at slow rotation rates and quiescent solutions and, together with dissolved O_2, may modify the oxide-growth dynamics on Pt (111) [37]. In this paper, the relation between initial oxidized states on Pt(111) and the ORR dynamics is assessed by employing electrochemical techniques, in order to get a deep insight about the interaction of oxygen, and the soluble intermediate, in these processes.

2. Experimental

Electrodes with (111) surface orientation were prepared from small Pt beads, approximately 2–3 mm in diameter, by the method described by Clavilier *et al.*[38]. All the experiments were performed in a two-compartment, three-electrode all-glass cell following a detailed experimental protocol [39]. Prior to each experiment, the electrodes were flame-annealed, cooled in a H_2/Ar atmosphere, and transferred to the cell

protected by a drop of ultrapure water saturated with H_2/Ar. Suprapure perchloric acid (Merck) was used to prepare the aqueous solutions in ultrapure water (Purelab Ultra, Elga-Vivendi). H_2, O_2, and Ar. (N50, Air Liquid) were also employed. All potentials were measured against the Reversible Hydrogen Electrode (RHE), and a large, flame-cleaned, Pt wire coil was used as a counter electrode.

Oxygen reduction on Pt (111) surfaces was studied under convective low regime by using the hanging meniscus rotating disk electrode (HMRDE) configuration [40]. For this purpose, an electrode holder for bead-type single-crystal electrodes was adapted to a Radiometer EDI-10K rotor. The electrode was placed in the holder so that its surface was perpendicular and centered to the rotation axis (as much as possible). Different Ar/O_2 ratios at a constant total pressure in the solution and the cell atmosphere with a total pressure ca. 1 bar were employed.

All voltammetric scans were collected at freshly annealed surfaces, cycled first in the low potential region to verify their quality, as well as the cleanliness of the surface, including each sweep rate change. The stability of the voltammetric profiles with time was also carefully checked to ensure solution cleanliness, especially during HMRDE experiments, owing to forced convection. *In situ* IR drop corrections were made, when necessary, to compensate the electrolyte resistance [41,42].

3. Results and discussion

3.1. The ORR dynamics at high potentials

Cyclic voltammetric profiles (CV's) for Pt(111) in oxygen-saturated, 0.1 M $HClO_4$ solutions, from 0.06 to 1.15 V, at room temperature and 0.05 V s^{-1} are shown in Figure 1A. At fast enough rotation rates, ~ $\omega > 200$ rpm, compared to the electrode scan rate, v, the CV displays the typical, *S*–shaped curve (steady state response), theoretically predicted for RDE systems [41]. In this case, the reaction onset is ca. 1.0 V, versus the reversible hydrogen electrode (RHE), and the limiting current, j_{lim}, is reached between 0.75 and 0.3 V. At E < 0.3 V, i.e. when hydrogen adsorption begins in the negative-going sweep (see Fig. 1), CV's show two current decays and H_2O_2 is detected [11, 43]. Because of that, jointly with the observation of a similar decrease in current during H_2O_2 reduction [29], it can be stated that adsorbed hydrogen, H_{ads}, may prevent O-O bond scission or block the relevant surface sites required for this process.

In contrast, at slow enough rotation rates, ~ $\omega < 200$ rpm, *j–E* curves exhibit two current peaks: one in the positive direction, j_{p1}, around 0.27 V, and other in the negative-going scan, j_{p2}, at ~0.85 V. While j_{p1} likely corresponds to H_2O_2 reduction, accumulated in the interface because of the reaction inhibition by H_{ads}, E_{H2O2}, the chemical nature of j_{p2} is unknown, E_{ORR}. At first glance, it could be said that this peak appears because of

the O_2-diffusion layer recovery at high potentials, where apparently there is no reaction. However, the dependence of j_{p2} on ω and the higher $j/|j_{lim}|$ ratio at 70 rpm than that observed at quiescent solutions around E_{ORR}, Fig. 1B, do not support this explanation. This is because during RDE experiments if the diffusion layer thickness is thinner than the steady value, δ_0, for a given ω, the current response should follow that for a stationary electrode (transient response), and the CV will display a peak, whose maximum magnitude, j_p, $\propto \delta_0^*$, regardless ω [41, 44–46].

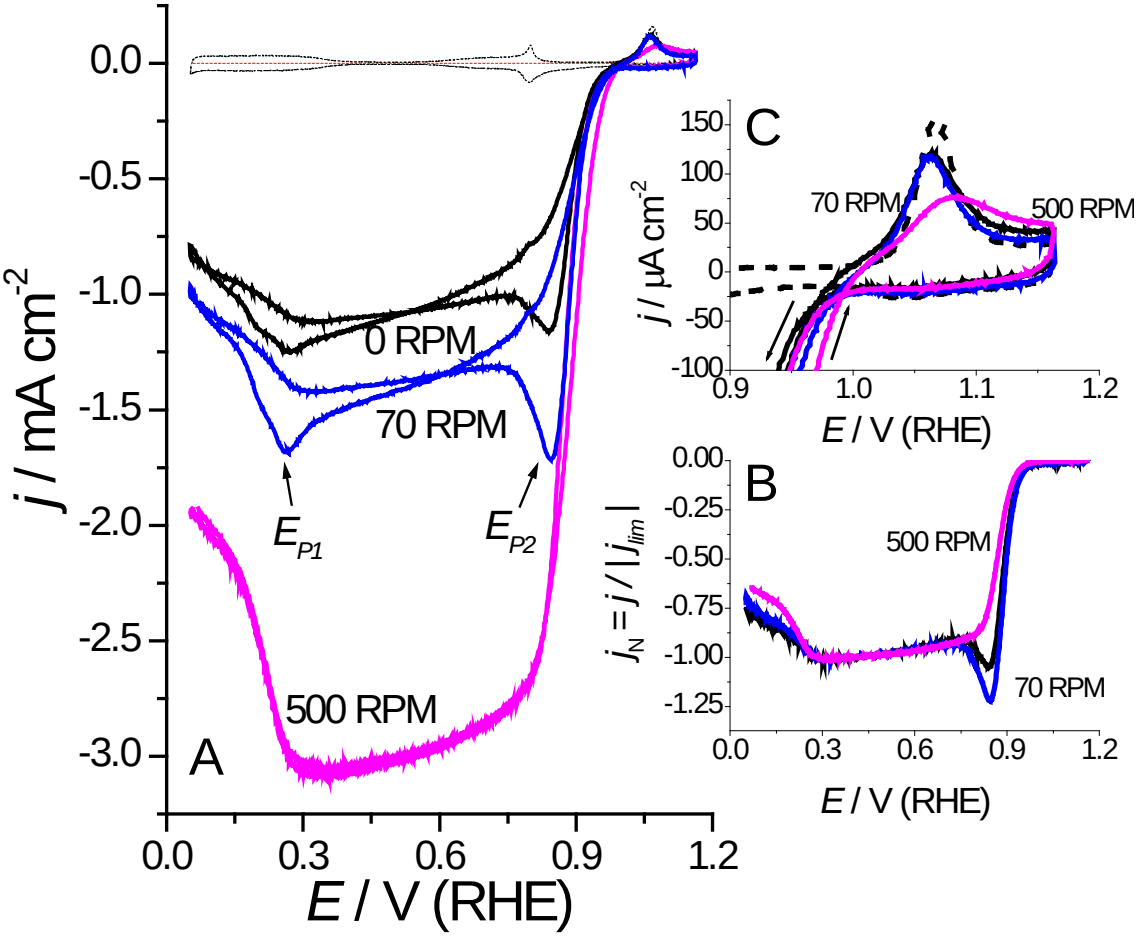

Fig. 1: Oxygen reduction on a HMRD Pt (111) electrode in O_2-saturated 0.1 M $HClO_4$ at 0, 70 and 500 rpm. Scan rate 0.05 V s^{-1}. A) CV profiles from 0.06 to 1.15 V. B) Negative-going scans normalized against limiting currents. C) Detailed view of the CV in the high potential region. Arrows indicate the direction of the scan.

Contrary to what is expected for an irreversible reaction [41, 46], at slow rotation rates j_{p2} depends on ω and $\propto \delta_0^*$. This only could be explained considering that the reacting species is not initially present in the solution, but it is produced as a product of a previous reduction of O_2, *i.e.* this species is a soluble intermediate [37]: at increasing ω the O_2-flux close to the electrode surface will also increase, and more molecules of the intermediate species could be produced, and even accumulated. At the same time, nevertheless, some molecules of the intermediate species will also diffuse fast away from the surface, avoiding the possibility of

charge transfer with the electrode. This complex balance would explain the measured dependence on ω of j_{p2}. This will be particularly important if non-covalent interaction with other water molecules close to the surface can take place [47–49], especially if the applied potential is close enough to the formal potential of this species.

After a mechanistic analysis, and similar to what has been reported for alkaline solutions [50], the formation, and subsequent reduction, of the soluble OOH* radical was suggested to be at the origin of E_{ORR} [37]:

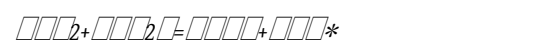

(1)

(2)

In this scheme, equation (1) is similar to the first chemical step in the ORR mechanism initially proposed long time ago by Damjanovic and Brusic [4], with the difference that OOH* is considered here to be dissolved, instead of adsorbed, as it was suggested by these authors. Of course, OOH* species can easily interact by hydrogen bonding with water molecules close to the electrode surface.

3.2. A scan rate study for the ORR

To clarify if E_{ORR} could be due to the reduction of a soluble species and get insight into its dynamics, cyclic voltammograms at different scan rates, oxygen concentrations and rotation rates were recorded. This is because in cyclic voltammetry [41, 46], changes in magnitude, j_p, and position, E_p, of a voltammetric peak when changing the scan rate can give information about the nature and kinetics of the electrochemical processes occurring at the interface [41]. Figures 2 and 3 resume selected *j*–*E* profiles, after subtracting the blank, in O_2-saturated, 0.1 M $HClO_4$ solutions at 70 and 500 rpm, respectively.

As explained above, in RDE experiments an electrochemical reduction peak appears in the voltammogram when the contribution of convection to the electrode dynamics becomes negligible. Then, the current response follows that expected for a stationary electrode under quiescent voltammetric conditions [43]. Consequently, a linear dependence on the square root of v is expected for j_p, when the reacting species is dissolved, with an intercept close to zero and a slope proportional to the transfer coefficient of the reactant. Besides, the position of E_p should also follow a linear dependence with the logarithm of v, and the slope would correspond to half of the Tafel slope for the reaction [41, 43].

Thus, from Figs. 2 and 3, it could be said that the reduction current at E_{H2O2} and E_{ORR} are compatible with an electrochemical reduction involving soluble species. This is because the dependence of j_p on $v^{½}$ at slow scan rates is linear, as depicted in Figs. 2C and 3C for E_{ORR}, suggesting diffusion controlled process at these v´s. However, fitted straight lines have a non-zero intercept and slopes are slightly different at 70 and 500 rpm.

Similar results were also obtained at lower O_2 concentrations. Thus, the reacting species should be different to dissolved O_2, and its concentration in the interface depends on many factors, such as v, ω, O_2 concentration, etc. At fast scan rates j_{p2}´s values are lower than expected because diffusion cannot cope with the charge transfer. In consequence, attempts to determine the reaction transfer coefficient from these data, inside the current theoretical framework, are meaningless.

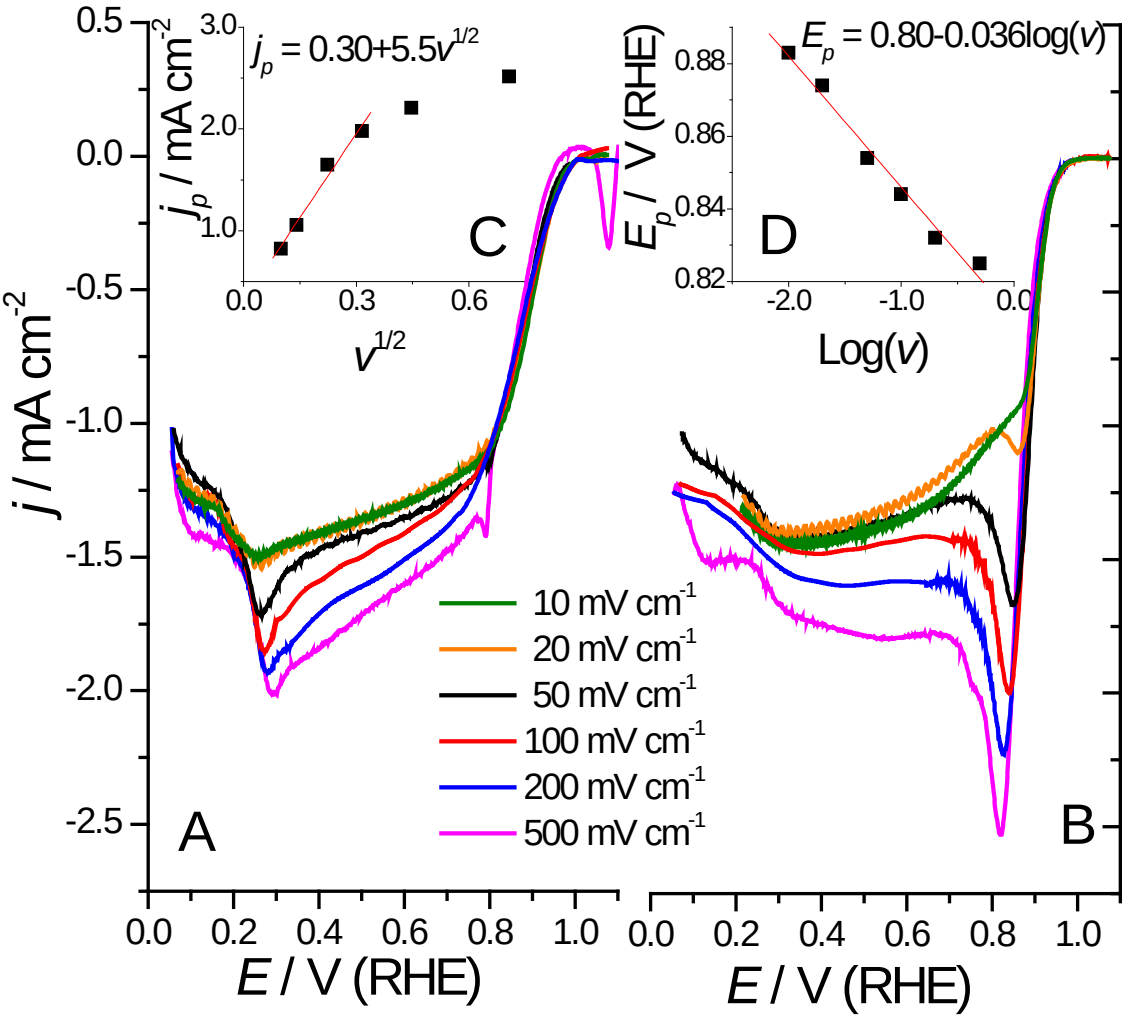

Fig. 2: Cyclic voltammograms, after subtracting the blank, on Pt (111) in O_2-saturated, 0.1 M $HClO_4$ solution at 70 rpm and different scan rates. A) Positive-going scan. B) Negative-going scan. C) Peak density current at higher potentials, j_{p2}, as a function of the squared root of the scan rate, $v^{½}$. D) Sweep-rate dependence of the E_{ORR}.

In contrast, the change in E_{ORR} with the logarithm of v does not depend on the rotation rate, Figs. 2D and 3D, or the O_2 concentration (data not shown), and fitted straight lines do have similar slopes and intercepts. Therefore, the Tafel slope for the ORR on Pt(111) can be approximate from these measurements and would be equal to two times the fitted slope in Figs. 2D and 3D [41, 44], *i.e.* between 62 to 72 mV. Besides, fitted

intercepts predict a current peak between 0.810 and 0.816 V at 1 V s^{-1}. Interestingly, both, the Tafel slope and E_{ORR} at 1 V s^{-1}, are close to experimental values determined from the analysis of Levich–Koutecky plots [10, 37, 43, 51–54], and measured E_{ORR} at 1 V s^{-1}, Figs. 3B and D (see also Fig. 4).

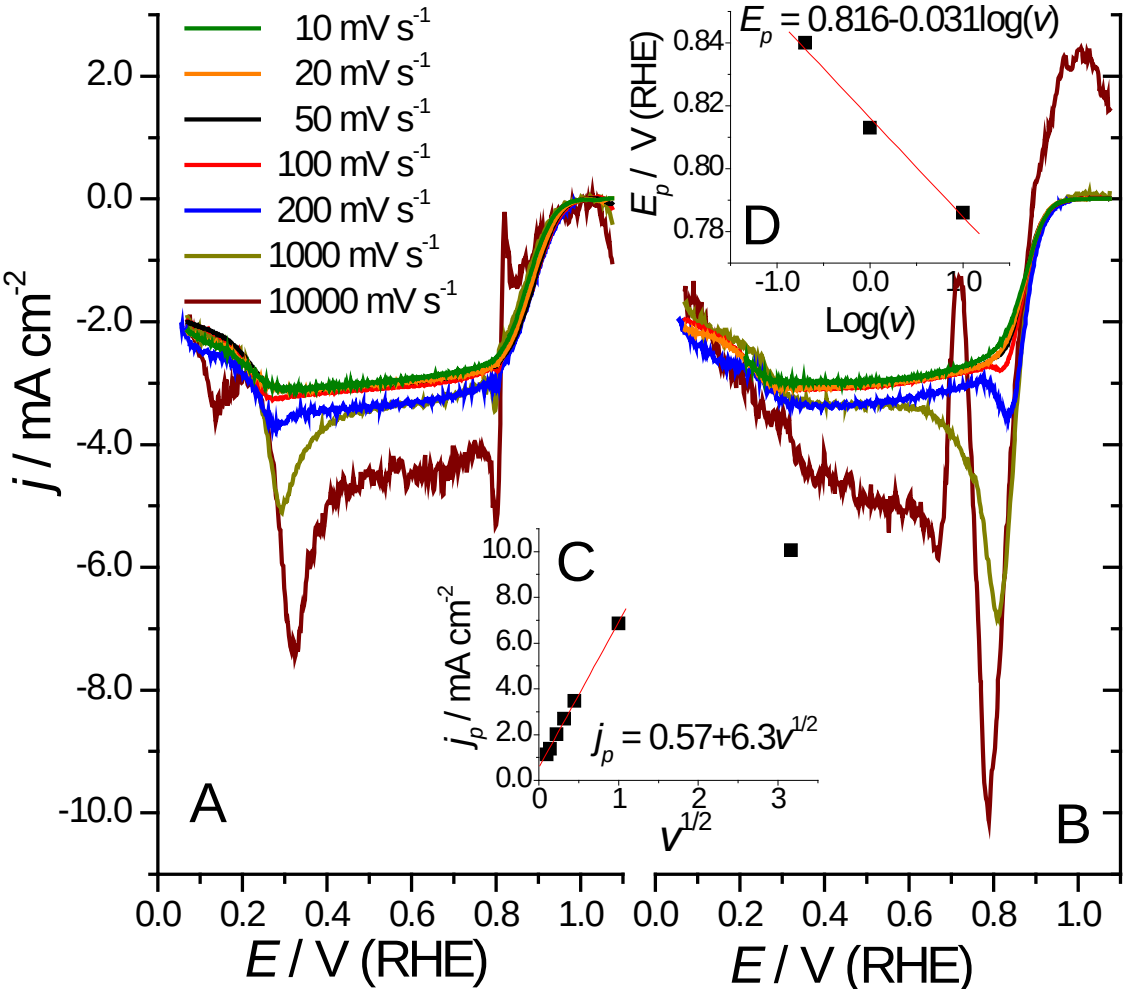

Fig. 3: Cyclic voltammograms, after subtracting the blank, on Pt (111) in O_2-saturated, 0.1 M $HClO_4$ solution at 500 rpm and different scan rates. A) Positive-going scan. B) Negative-going scan. C) Peak density current at higher potentials, j_{p2}, as a function of the squared root of the scan rate, $v^{½}$. D) Sweep-rate dependence of the E_{ORR}.

A deep analysis of these experimental results reveals that not only j_{p2} depends on ω, but also the apparent diffusion coefficient inside the diffusion layer, D_0, depends on ω and v. This latter condition is evident when the tail in the descending part of E_{ORR} is modeled by employing the Cottrell equation to calculate the expected current decay for a pure diffusive process and estimate the apparent Cottrell constant of the reacting species in solution, *B*. This was done not only at 0.05 V s^{-1} but also at 0.2 and 1 V s^{-1}, and different rotation rates, as shown in Figure 4.

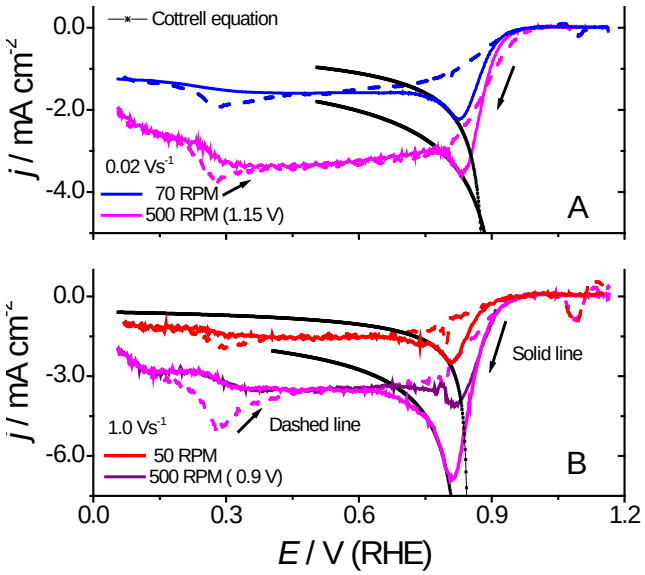

Fig. 4: Cyclic voltammograms, after subtracting the blank, on Pt (111) in O_2-saturated, 0.1 M $HClO_4$ solution and fitted Cottrell curves for each case. A) Scan rate 0.2 V s^{-1}, 70 and 500 rpm. B) Scan rate 1 V s^{-1}, 50 and 500 rpm.

Under this framework, the decrease in current beyond the peak does not depend on E but on $t^{-½}$, according to [55, 56]:

$$j = B(E_0 - E) \quad (3)$$

in which E_0 is an hypothetical origin in the j–E curve which matches the diffusion part of the voltammogram and B, the Cottrell constant, given by [55]:

$$B = 0.62 n F A D_0^{2/3} \nu^{-1/6} \omega^{1/2} C_0^* \quad (4)$$

C_0^* the solution concentration and D_0 the diffusion coefficient of the reacting species.

As seen in Fig. 4, although calculated Cottrell curves fit well the descending part of current peaks, suggesting the existence of diffusion controlled processes, estimated parameters depend on ω and ν, table 1. Moreover, estimated parameters are also different from theoretical values calculated for dissolved O_2, which would be $B = 0.62 n F A D_0^{2/3} \nu^{-1/6} C_0^*$ follows the expected tendency, Figs. 2C and 3C, the Cottrell constant dependence on ω and ν suggests that the apparent diffusion coefficient inside the diffusion layer, D_0, also depends on ω and ν, which C_0^* and D_0 for the reacting species at E_{ORR}.

Table 1: Estimated Cottrell parameters for ORR at different scan and rotation rates

Scan rate / Rotation rate	0.05 V s^{-1}		0.2 V s^{-1}		1 V s^{-1}	
	$E°$ (V)	B ($s^{½}$)	$E°$ (V)	B ($s^{½}$)	$E°$ (V)	B ($s^{½}$)
50 rpm	0.94	2.24			0.85	0.53
70 rpm	0.93	2.21	0.89	1.34		

500 rpm			0.94	2.65	0-84	1.35

3.3. Interplay between initial oxidized states on Pt(111) and the ORR dynamics

In addition to the possible existence of a soluble intermediate species, results in Fig. 1 also do not support the poisoning role on the ORR by OH_{ads} and/or O_{ads}, commonly claimed [11–22]. First, because the difference in current between positive and the negative-going scans close to the foot of the ORR wave, Fig 1C, usually interpreted as a proof of ORR inhibition by O_{ads} [10, 52], disappears at fast scan rates, although the formation of OH_{ads} and O_{ads} have already taken place [33, 36], as can be seen in Fig. 4B. Thus, adsorbed oxygen-containing species should not be responsible of this difference in current between both scans at 0.05 V s^{-1} [37].

Second, contrary to what is expected from an inhibiting role of OH_{ads} and/or O_{ads}, at slow rotation rates, potential excursions to high potentials, *i.e.* E_{up} = 1.15 V, where a higher O_{ads} coverage is attained [33, 36], define a rotation-rate dependent peak in the negative-going scan. This peak has greater reduction currents between 0.9 and 0.75 V than those measured if lower upper potential limits were employed, *i.e.* E_{up} = 0.9 V, where a lower O-containing species coverage is reached [33, 36], Figs. 4B. Thus, higher O_{ads} coverages can apparently enhance the electrode activity toward the ORR, totally opposing to the poisoning role long claimed, and similar to what has been recently suggested from X-ray photoelectron spectroscopy in fuel cell cathodes [57]. Nevertheless, it should be stressed that dissolved oxygen modifies the dynamics of the initial states in the oxide growth process on Pt(111), apparently acting like an extra O_{ads} source [37], Fig. 1C.

In order to evaluate the role of oxygenated species from the Pt(111) oxidation process, results should be compared with similar experiments in O_2-free solutions. In this case, the system has been electrochemically well characterized, and results from past studies will be briefly summarized below [33, 58–60]. In 0.1 M $HClO_4$ solutions the CV on Pt(111) is characterized by three zones, Figure 5. At E < ~0.35 V, hydrogen adsorption/desorption, H_{ads}, takes place. Between ca. 0.35 to 0.6 V there is a flat, pseudo-double layer region [58, 60]. At higher potentials, the adsorption of O-containing species occurs by a sequential electrochemical oxidation of water, through two interrelated processes: the reversible formation of hydroxide OH_{ads}, in the so-called “butterfly” region, between 0.6 to 0.85 V, $E_{1p,B}$ and $E_{1p,S}$, given by [33, 59]:

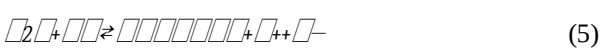

(5)

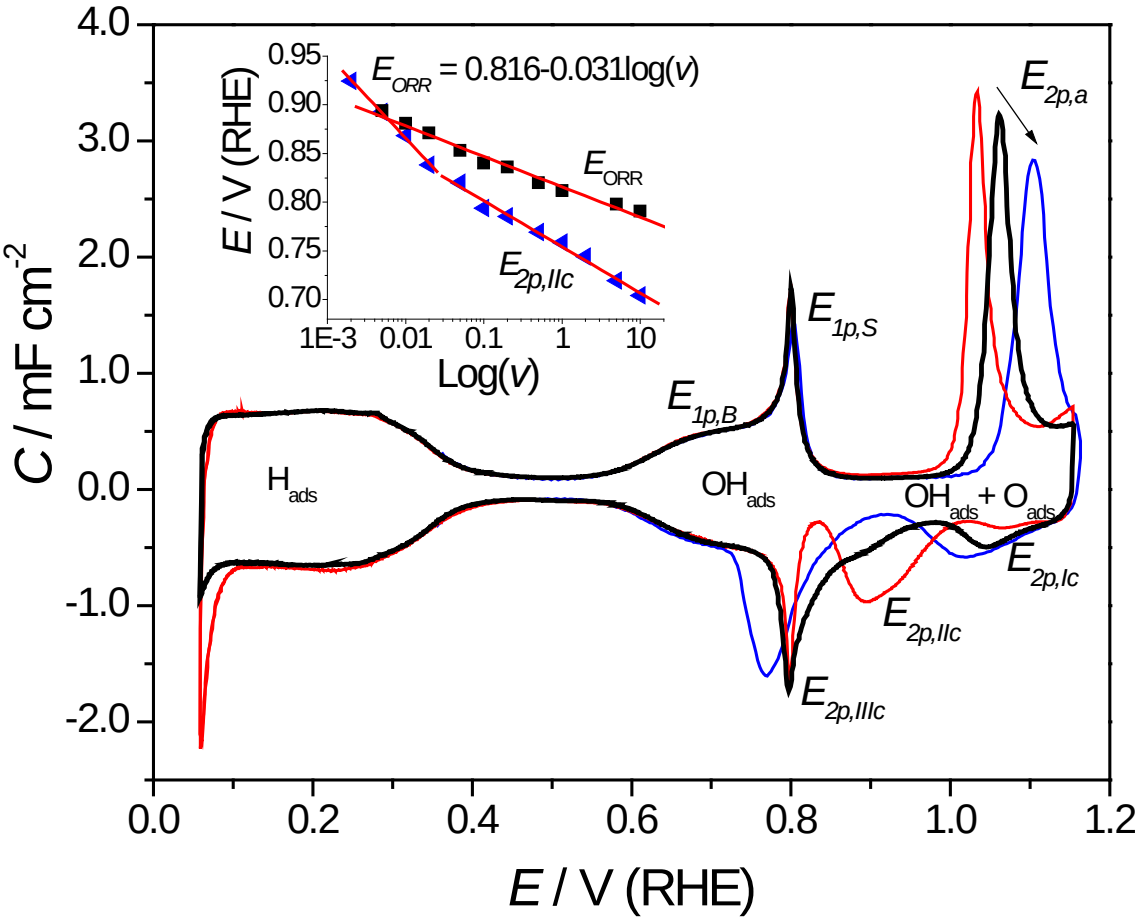

Fig. 5: Stable voltammetric profile of a Pt(111) in 0.1 M $HClO_4$ solution between 0.06 and 1.15 V at 0.005, 0.05 and 0.5 V s^{-1} [33]. Inset: Sweep-rate dependence of the peak potentials for the ORR, E_{ORR}, and the reduction of the second oxidation peak, $E_{2p,IIc}$, on Pt(111) in O_2-saturated and O_2-free solutions, respectively.

and its subsequent oxidation to O_{ads}, at $E > 1.0$ V, $E_{2p,a}$, according to [33, 59]:

□□□□□□□⇄□□□□□□□+□++□− (6)

During these initial states of the oxide growth process on Pt(111), the nature and coverage of adsorbed species are determined by the structure of the adlayer. In this sense, once the "butterfly" is completed (0.9 V), a mixed OH_{ads}/water is adsorbed onto the surface, while the surface composition between $1.0 < E < 1.15$ V involves mixed OH_{ads}/O_{ads}/water layers, in which the ratio between the coverage of adsorbed species changes as a function of the potential and scan rate, v, until a stable layer is formed [33, 59]. In parallel, formed O_{ads} slowly converts to PtO. Hence, at different scan rates the ORR would occur over a surface with different OH_{ads} and O_{ads} coverages, because at slow v the O_{ads} coverage on the surface will be higher, and the OH_{ads} coverage smaller, than at faster v [33].

In the negative-going scan, $E_{2p,a}$ desorbs through three stages: a reversible contribution, attributed to OH_{ads} adsorbed at high potentials, $E_{2p,Ic}$, and two irreversible features: $E_{2p,IIc}$ and $E_{2p,IIIc}$ assigned to the reduction of

O_{ads} and PtO species, respectively [33, 59], Fig. 5. Instead, $E_{1p,B}$ and $E_{1p,S}$ should reversibly desorb, as long as $v < 10$ V s^{-1} [33].

If the change in $E_{2p,IIc}$ and E_{ORR} vs. log. v, in O_2-free and O_2-saturated solutions, are compared, inset to Fig 5, it can be seen that these processes have different electrochemical dynamics. While $E_{2p,IIc}$ shows two linear tendencies: at $v < 0.02$ V s^{-1} and at faster v, with slopes of 0.078 and 0.047 V dec^{-1}, respectively, E_{ORR} only evidences one linear tendency, with a slope ~0.031 to 0.036 V dec^{-1}, Figs. 2D and 3D. Thus, for most sweep rates, E_{ORR} occurs over an oxidized surface, *i.e.* before than $E_{2p,IIc}$ and $E_{1p,B}$ and $E_{1p,S}$ reduction processes have taken place. Only at $v \geq 1$ V s^{-1} E_{ORR} takes place in the same potential region where OH_{ads} desorbs. Moreover, solely at v < 0.005 V s^{-1}, E_{ORR} appears after O_{ads} desorption, but before OH_{ads} reduction. Therefore, according to these results, neither OH_{ads} nor O_{ads} should inhibit the ORR dynamics, because the reaction dynamics does not change despite the change in OH_{ads} and O_{ads} coverages.

Finally, as can be appreciated from Figs. 2 and 3, besides E_{H2O2} and E_{ORR}, CVs at different scan rates do not shown any distinctive current contribution from an adsorbed species. Thus, it is expected that this system does not involve any other adsorbed species, or a different O-containing species coverage, distinct from the adsorbates already occurring at the Pt(111) surface in absence of oxygen: *i.e.* the surface coverage corresponding to bulk oxygen reaction intermediates is negligible. This result is similar to what was suggested from impedance experiments, in which similar 2D-adsorbed structures in O_2-free and O_2-saturated solutions were proposed [61]. In this sense, any theoretical model predicting higher surface coverages than those present at the surface in absence of oxygen should be reevaluated [14, 62].

3.4. Role of OH_{ads}/O_{ads} in the ORR dynamics on Pt(111)

Theoretically, it has been shown that bonding of O_2, OOH* and H_2O_2 to Pt surfaces decreases the high activation energies for these outer–sphere reductions [63–65], but at the same time increases HO* activation energy [63] and stabilises OH_{ads} and O_{ads} [12, 13, 66–70]. Because of that, the formation of OOH_{ads}, compared to O_{ads} + OH_{ads}, would not be stable [67], and so, the reduction of this species, if formed, would occur in the solution side of the interface. Only at high potentials, when Pt–OH and Pt–O bounds are weakened, due to the increase in the O_{ads} coverage [59, 67, 71], OOH* could adsorb and reduce but, at these potentials, formed H_2O_2 will rapidly decompose to O_2 [28–30], leading to a total zero current at those potentials in this potential region, as expected from experimental results.

If the reduction of OOH* (and H_2O_2) on metallic surfaces were considered to occur as a Fenton type reaction [72], experimental results reported here could be explained. In this sense, there would be a complex

relationship between competing species on, or close to, the electrode surface. At high potentials, surface oxides would act as a "redox mediator" of the ORR through the PtOH/PtO redox system, similar to what has been proposed for H_2O_2 oxidation and reduction reactions [28]. Hence, analogous to Fenton type reactions [72], reactions close to the electrode surface would be:

$\square_2\square_2 = \square\square\square + \square_2\square + \square\square *$ $\Delta G_0 \approx 0.06$ eV (7)

$\square * + \square_2\square_2 = \square_2\square + \square\square\square *$ $\Delta G_0 \approx -1.61$ eV (8)

$\square * = \square\square\square + \square_2\square$ $\Delta G_0 \approx -1.71$ eV (9)

$\square * = \square\square\square + \square_2\square_2$ $\Delta G_0 \approx -0.58$ eV (10)

$\square * = \square\square\square\square + \square_2$ $\Delta G_0 \approx -1.06$ eV (11)

In these equations ΔG_0s are given as reference values and they were estimated using standard reversible potentials [64, 65] and calculated ΔG_{ads} for adsorbed species. It has been shown that applying these approximations the error bars in predicted ΔG_0´s values are ± 0.1 eV or less [73]. Eqns. 10 and 11 represent the OOH* dismutation, mediated by the metal, whose extent will depend on $[H_2O_2]/[O_2]/[PtOH]/PtO$ ratios and the solution pH. At the same time, the overall process would depend on the competition between those steps, water dissociation reactions and the [PtOH]/[PtO] ratio. Interestingly, the existence of a radical intermediate species would explain the sensitivity to solution impurities of the ORR on platinum [3, 74, 75].

Recent attention in electro-catalyst improvement has focused on the development of platinum alloys with nano-structured compositional gradients that exhibit higher activity than supported Pt nano-particles [6, 15, 76–78]. However, from the above results, a new approach for electro-catalyst development is suggested and more research efforts are necessary to clarify the relationship between ORR activity improvements, changes in the surface oxidation dynamics and the reducing properties toward OOH* and H_2O_2 of new materials.

3.5. Pt(111) oxide and the ORR

To finish, it would be important to discuss the effect of potential excursions at values higher than 1.15 V. It has been reported that [79] the O-containing species coverage on Pt(111) increases over 1 electron per Pt atom at potentials higher than 1.15 V, and consequently the formation of PtO species should occur. This process involves surface disordering and the electrode structure will not correspond to that of a well-ordered {111} facet any more. Figure 6A depicts the high potentials region of CVs in O_2-saturated 0.1 M $HClO_4$ solutions at two different upper potential limits, E_{up}, 1.15 and 1.60 V. From this figure, it can be seen that, despite the lack of reduction current at high potentials, dissolved oxygen interacts with the electrode surface and not only modifies the OH_{ads} and O_{ads} adsorption processes, Fig. 1C, but also the PtO formation.

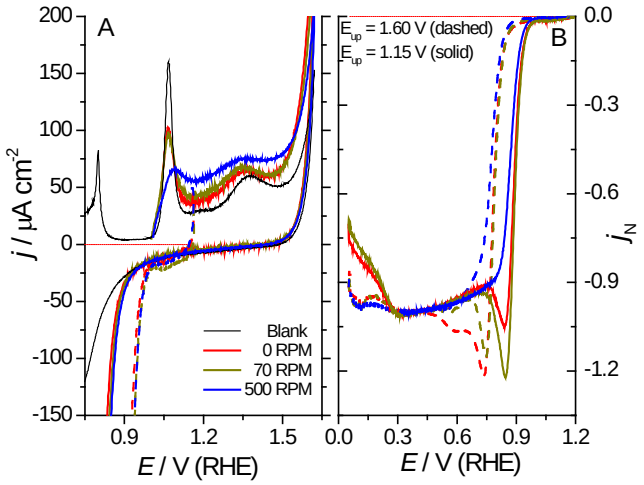

Fig. 6: A) Detailed view in the high potential region of cyclic voltammograms of Pt (111) in O_2-saturated 0.1 M $HClO_4$ solution at two different upper potential limits: E_{up} = 1.15 V and 1.60 V. B) Normalized negative-going scans after potential excursions to E_{up} = 1.15 V and 1.60 V. Scan rate 0.05 V s^{-1}.

In addition, Fig 6A shows that in O_2-saturated solutions, the oxygen evolution reaction (OER) occurs at higher reaction rates than without oxygen in the solution. This result could support the theoretical view about the necessity of a critical O_{ads} coverage for the formation of superoxide-type (OOH) species, considered to be the slow step in the water splitting process [67]. However, in disordered surfaces this is not the case, and oxidation rates in both O_2-free and O_2-saturated solutions are almost the same, Figure 7A. Nevertheless, at disordered surfaces the OER already begins ~70 mV less positive than in ordered ones.

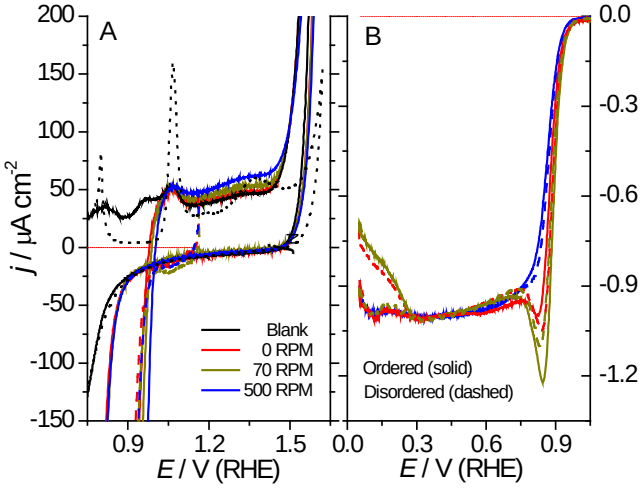

Fig. 7: A) Detailed view in the high potential region of cyclic voltammograms of disordered Pt (111) in O_2-saturated 0.1 M $HClO_4$ solution at two different upper potential limits: E_{up} = 1.15 V and 1.60 V. B) Normalized negative-going scans after potential excursions to E_{up} = 1.15 V and 1.60 V. Scan rate 0.05 V s^{-1}.

In contrast to results discussed in past sections regarding OH_{ads} and O_{ads} coverages, the ORR is inhibited during the negative-going scan after potential excursions at E_{up} = 1.60 V, and only can occur once the reduction of adsorbed PtO species takes place, Fig. 6B. In this case, the poisoning role of PtO species on the ORR reaction is clear. However, in the next voltammetric cycle, after PtO has desorbed, the ORR on the new disordered surface is slightly faster than on a well ordered electrode, provided an E_{up} < 1.15 V, Fig. 7B. Again, it is remarkable that hydrogen adsorption on disordered surfaces does not inhibit ORR unless potentials close to hydrogen evolution are reached.

4. Conclusions

In this paper, the reduction of oxygen on Pt(111) in the high potential region is analyzed by using electrochemical techniques, such as hanging meniscus cyclic voltammetry in quiescent solutions and under rotating disk regime. A scan rate study analysis of the reduction peak that appears at high potentials, E_{ORR}, is assigned to the reduction of the intermediate involved in the ORR rate determining step. Results suggest that neither OH_{ads} nor O_{ads} inhibit the reaction, as commonly believed, and so these species should not be the main bottleneck in the mechanism. In contrast, oxide species, PtO, formed at potentials even higher where surface reordering can take place, strongly inhibit the ORR, which only can take place once the reduction of PtO begins.

In addition, the dependence on ω of the current maximum, j_{p2}, which implies that the concentration of reacting species depends on ω, and the dependence on ω and v of the apparent diffusion coefficient of the reacting species is consistent with the formation of a soluble intermediate species at the origin of E_{ORR}.

Acknowledgments

This study has been carried out in the framework of the European Commission FP7 Initial Training Network ‘‘ELCAT’’, Grant Agreement No. 214936–2. Support from the Spanish MICYNN though project CTQ2013–44083-P and GV through PROMETEOII/2014/013 (FEDER) are greatly acknowledged.

References

1. Wroblowa HS, Chi PY, Razumney G (1976) J Electroanal Chem 69:195.
2. Kinoshita K (1992) Electrochemical Oxygen Technology, John Wiley and Sons, New York.
3. Damjanovic A, Genshaw MA, Bockris JOM (1966) J Phys Chem 70:3761.
4. Damjanovic A, Brusic V (1967) Electrochim Acta 12:615.
5. Appleby AJ (1970) Catal Rev 4:221.
6. Mukerjee S, Srinivasan S, Soriaga MP, McBreen J (1995) J Electrochem Soc 142:1409.

7. Llang CC, Juliar AL (1965) J Electrochem Chem 9:390.
8. Damjanovic A, Brusic V (1967) Electrochim Acta 12:615.
9. Paucirova M, Drazic DM, Damjanovic A (1973) Electrochim Acta 18:945.
10. Markovic NM, Adzic RR, Cahan BD, Yeager EB (1994) J Electroanal Chem 377:249.
11. Markovic NM, Ross PN Jr (2002) Surf Sci Rep 45:117.
12. Nørskov J, Rossmeisl J, Logadottir A, Lindqvist L (2004) J Phys Chem B 108:17886.
13. Viswanathan V, Hansen H, Rossmeisl J, Nørskov JK (2012) ACS Catal 2:1654.
14. Jinnouchi R, Kodama K, Hatanaka T, Morimoto Y (2011) Phys Chem Chem Phys 13: 21070.
15. Stamenkovic VR, Fowler B, Mun BS, Wang G, Ross PN, Lucas CA, Markovic NM (2007) Science 315:493.
16. Roques J, Anderson AB, Murthi VS, Mukerjee S (2005) J Electrochem Soc 152:E193.
17. Mukerjee S, Srinivasan S, Soriaga MP, McBreen J (1995) J Phys Chem 99:4577.
18. Teliska M, Murthi VS, Mukerjee S, Ramaker DE (2005) J Electrochem Soc 152:A2159.
19. Markovic NM, Gasteiger HA, Ross PN Jr (1996) J Phys Chem 100:6715.
20. Schmidtz TJ, Stamenkovic V, Ross PN Jr, Markovic NM (2003) Phys Chem Chem Phys 5:400.
21. Markovic NM, Gasteiger HA, Grgur BN, Ross PN (1999) J Electroanal Chem 467:157.
22. Wang JX, Markovic NM, Adzic RR (2004) J Phys Chem B 108:4127.
23. Wakisaka M, Suzuki H, Mitsui S, Uchida H, Watanabe M (2008) J Phys Chem C 112:2750.
24. Attard GA, Ye JY, Brew A, Morgan D, Bergstrom-Mann P, Sun G (2014) J Electroanal Chem 716:106.
25. Shao M, Sasaki K, Marinkovic NS, Zhang L, Adzic RR (2007) Electrochem Commun 9:2848.
26. Strmcnik D, Escudero–Escribano M, Kodama K, Stamenkovic VR, Cuesta A, Marković NM (2010) Nat Chem 2:880.
27. Balbuena PB, Calvo RS, Lamas EJ, Salazar PF, Seminario JM (2006) J Phys Chem B 110:17452.
28. Katsounaros I, Schneider WB, Meier JC, Benedikt U, Biedermann PU, Auer AA, Mayrhofer KJJ (2012) Phys Chem Chem Phys 14:7384.
29. Gómez-Marín AM, Schouten KJP, Koper MTM, Feliu JM (2012) Electrochem Commun 22:153.
30. Katsouraros I, Schneider B, Meier JC, Benedikt U, Biedermann PU, Auer AA, Cuesta A, Mayrhofer KJJ (2013) Phys Chem Chem Phys 15:8058.
31. Tian F, Anderson AB (2011) J Phys Chem C 115:4076.
32. Walch SP (2011) J Phys Chem C 115:7377.

33. Gómez–Marín AM, Clavilier J, Feliu JM (2013) J Electroanal Chem 688:360.

34. Shao M, Sasaki K, Marinkovic NS, Zhang L, Adzic RR (2007) Electrochem Commun 9:2848.

35. Teliska M, Murthi VS, Mukerjee S, Ramaker DE (2007) J Phys Chem C 111:9267.

36. Wakisaka M, Suzuki H, Mitsui S, Uchida H, Watanabe M (2009) Langmuir 25:1897.

37. Gómez–Marín AM, Feliu JM (2013) ChemSusChem 6:1091.

38. Clavilier J, Armand D, Sun S, Petit M (1986) J Electroanal Chem 205:267.

39. Korzeniewsky C, Climent V, Feliu JM (2012) Electroanalytical Chemistry A Series of Advances Vol 24 (Eds: Bard AJ, Zoski CG) CRC Press, Boca Raton, Chap 2, pp 75.

40. Cahan BD, Villullas HM (1991) J Electroanal Chem 307:263.

41. Bard AJ, Faulkner LR (2001) Electrochemical Methods: Fundamentals and Applications, 2nd ed, John Wiley and Sons, New York.

42. Van der Vliet D, Strmcnik DS, Wang C, Stamenkovic VR, Markovic NM, Koper MTM (2010) J Electroanal Chem 647:29.

43. Markovic NM, Gasteiger H, Ross PN Jr (1997) J Electrochem Soc 144:1591.

44. Andricacos PC, Cheh HY (1981) J Electroanal Chem 124:95.

45. Quintana GC, Andricacos PC, Cheh HY (1983) J Electroanal Chem 144:77.

46. Andricacos PC, Cheh HY (1980) J Electrochem Soc 127:2173.

47. Sandoval AP, Gómez–Marín AM, Suárez–Herrera MF, Climent V, Feliu JM (2015) Submitted.

48. Strmcnik D, Kodama K, Van der Vliet D, Greeley J, Stamenkovic VR, Markovic NM (2009) Nat Chem 1:466.

49. Gohda Y, Schnur S, Groß A (2008) Faraday Discuss 140:233.

50. Shao M, Liu P, Adzic RR (2006) J Am Chem Soc 128:7408.

51. Macia MD, Campiña JM, Herrero E, Feliu JM (2004) J Electroanal Chem 564:141.

52. Kuzume A, Herrero E, Feliu JM (2007) J Electroanal Chem 599:333.

53. Pérez J, Villullas HM, Gonzalez ER (1997) J Electroanal Chem 435:179.

54. El Kadiri E, Faure R, Durand R (1991) J Electroanal Chem 301:177.

55. Climent MA, Aldaz A, Vásquez JL (1983) Anal Quim 79:660.

56. Bontempelli G, Magno F, Daniele S (1985) Anal. Chem. 57:1503.

57. Norskov JK, Nilsson A, Ogasawara H (2013) Nat Commun 4:2817.

58. Clavilier J, Rodes A, El Achi K, Zamakhchari MA (1991) J Chim Phys 88:1291.

59. Gómez–Marín AM, Feliu JM (2013) Electrochim Acta 104:367.

60. Berná A, Climent, V, Feliu JM (2007) Electrochem Commun 9:2789.

61. Bondarenko AS, Stephens IEL, Hansen HA, Pérez-Alonso FJ, Tripkovic V, Johansson TP, Rossmeisl J, Nørskov JK, Chorkendorff I (2011) Langmuir 27:2058.

62. Hansen, HA, Viswanathan V, Nørskov JK (2014) J Phys Chem C 118:6706.

63. Anderson AB, Albu TV (2000) J Electrochem Soc 147:4229.

64. Anderson AB, Albu TV (1999) Electrochem Commun 1:203.

65. Anderson AB, Albu TV (1999) J Am Chem Soc 121:11855.

66. Rossmeisl J, Karlberg GS, Jaramillo T, Nørskov JK (2008) Faraday Discuss 140:337.

67. Rossmeisl J, Logadottir A, Nørskov JK (2005) Chem Phys 319:178.

68. Karlberg GS, Rossmeisl J, Nørskov JK (2007) Phys Chem Chem Phys 9:5158.

69. Tripkovic V, Skulason E, Siahrostami S, Nørskov KJ, Rossmeisl J (2010) Electrochim Acta 55:7975.

70. Hansen HA, Rossmeisl J, Nørskov JK (2008) Phys Chem Chem Phys 10:3722.

71. Mooney CE, Anderson LC, Lunsford JH (1993) J Phys Chem 97:2505.

72. Koppenol WH (2001) Redox Report 6:229.

73. Anderson AB (2012) Phys Chem Chem Phys 14:1330.

74. Scherson DA, Tolmachev YV (2010) Electrochem Solid-State Lett 13:F1.

75. Damjanovic A, Genshaw MA, Bockris JOM (1967) J Electrochem Soc 114:466.

76. Nilekar AU, Mavrikakis M (2008) Surf Sci 602:L89.

77. Markovic NM, Schmidt TJ, Stamenkovic V, Ross PN (2001) Fuel Cells 1:105.

78. Stamenkovic V, Mun BS, Mayrhofer KJJ, Ross PN, Markovic NM, Rossmeisl J, Greeley J, Nørskov JK (2006) Angew Chem Int Ed 45:2897.

79. Gomez-Marin AM, Feliu JM (2012) Electrochim Acta 82:558.